OHSTPY-HEP-T-00-004
GUPTA/00-06-06
CLNS 00-1678

Scaling and Further Tests of Heavy Meson Decay Constant Determinations from NRQCD

S.Collins[a*], C.T.H.Davies[a*], J.Hein[b], G.P.Lepage[b], C.J.Morningstar[c], J.Shigemitsu[d], J.Sloan[e†]

[a]Department of Physics & Astronomy, University of Glasgow, Glasgow, G12 8QQ, UK.

[b]Newman Laboratory of Nuclear Studies, Cornell University, Ithaca, NY 14853, USA.

[c]Department of Physics, Florida International University, Miami, FL 33199, USA

[d]Physics Department, The Ohio State University, Columbus, OH 43210, USA.

[e]Physics Department, University of Kentucky, Lexington, KY 40506, USA.

Abstract

We present results for the B_s meson decay constant f_{B_s} from simulations at three lattice spacings in the range a^{-1}= 1.1GeV to 2.6GeV using NRQCD heavy quarks and clover light quarks in the quenched approximation. We study scaling of this quantity and check consistency between mesons decaying from rest and from a state with nonzero spatial momentum. Cancellation of power law contributions that arise in the NRQCD formulation of heavy-light currents is discussed. On the coarsest lattice the D_s meson decay constant f_{D_s} is calculated. Our best values for the decay constants are given by $f_{B_s} = 187(3)(4)(12)(2)(8)(6)$ MeV and $f_{D_s} = 223(6)(29)(38)(23)(9)(^{+3}_{-1})$ MeV.

PACS numbers: 12.38.Gc, 13.20.He, 13.20.Fc

*UKQCD Collaboration

†Present address: Spatial Technologies, Boulder, CO, USA.

I. INTRODUCTION

The B meson decay constant, f_B, defined through the hadronic matrix element

$$\langle 0 \,|\, A_\mu \,|\, B,\, \vec{p}\,\rangle = p_\mu f_B, \tag{1}$$

is one of the phenomenologically relevant quantities whose determination has relied heavily on lattice calculations. Together with the bag-parameter B_B, the decay constant is an important ingredient in analyses of $B^0\overline{B^0}$ mixing phenomena and studies of CP violation in the neutral B system. Several quenched lattice determinations of f_B have been completed in recent years using different approaches to simulating the heavy b-quark on the lattice [1–8]. The first dynamical results are also starting to appear [9–11,6]. The most extensive quenched studies have been carried out using either the non-relativistic (NRQCD) formulation [12] or the heavy clover approach [13] to b-quarks. Results for f_B and f_{B_s} from these two methods are in good agreement with each other.

In this article we investigate once again the NRQCD approach to leptonic decays of heavy mesons. We wish to gain further insight into this method, which will strengthen confidence in our previous results and also allow us to assess its potential when going on to other important areas of heavy quark physics such as semi-leptonic decays. Our analysis is based on quenched results for the B_s meson decay constant from simulations at three lattice spacings spanning a^{-1} = 1.1GeV - 2.6GeV. We use NRQCD b-quarks, clover light quarks and the Wilson plaquette gauge action. Simulation parameters are summarized in Table I. The $\beta = 6.0$ f_{B_s} results in sections III & IV are taken from reference [3]. The configurations at $\beta = 5.7$ and $\beta = 6.2$ plus the light propagators at $\beta = 6.2$ were provided by the UKQCD collaboration. The $\beta = 6.0$ data presented in section VI also uses UKQCD configurations and light propagators. Some preliminary results at earlier stages of this project have appeared in [18,19].

Our first goal was to check for independence of our final f_{B_s} value from the lattice spacing used. This is particularly important here, since we employ an effective theory, NRQCD, for heavy quarks which precludes extrapolations to zero lattice spacing, $a \to 0$. There are many advantages to NRQCD, including being able to simulate quarks with masses much larger than the cutoff ($aM_Q \gg 1$) without introducing large discretization errors and the efficiency with which heavy quark propagators can be computed numerically. However, the theory is not renormalizable and furthermore aM_Q cannot become too small. In order for the approach to work, one must have a window in which the lattice spacing is large enough so that aM_Q is of $O(1)$ or greater, but also small enough so that all discretization errors, including those coming from the glue and light quark sectors, are under control. Physical results must already be independent of the lattice spacing within acceptable and quantifiable systematic errors. The scaling studies presented in this article demonstrate that such a window does indeed exist between $a^{-1} = 1.1 \sim 2.6$ GeV for simulations with NRQCD-clover quarks and Wilson glue. The systematic errors are $\sim 10\%$ in the upper half of the window and increase to $15 \sim 20\%$ towards the coarse end. By further improving the quark and gauge actions one should be able to improve the errors at the coarse end and even extend the window down below 1GeV. Recently the JLQCD/Hiroshima collaboration [4] studied scaling of f_B and

f_{B_s} with a lattice action very similar to the one used in this article. Our results are in good agreement with theirs.

Another feature of the use of an effective theory, is that the matrix element of current operators in the full theory (continuum QCD) such as the LHS of eq.(1) must be built up out of several current matrix elements evaluated in the effective theory,

$$\langle A_\mu \rangle_{QCD} = \sum_j C_j \, \langle J_\mu^{(j)} \rangle_{eff}. \tag{2}$$

With NRQCD heavy quarks the currents are of the form,

$$J_\mu^{(j)} = \frac{1}{(M_Q)^{l_j}} O_\mu^{(j)}, \tag{3}$$

where the $O_\mu^{(j)}$ are operators of dimension $d_j = 3 + l_j$ ($l_j \geq 0$). Quantum corrections to the currents and the mixing of higher dimension operators back onto lower dimension operators will induce "power law" terms, i.e. terms that go as $\alpha_s/(aM_Q)^{\delta l_j}$ (plus higher orders). Since the LHS of eq.(2) should have no power law contributions, any consistent framework for evaluating $\langle J_\mu^{(j)} \rangle_{eff}$ and C_j must arrange for power law terms to cancel to the order one is working in. The second goal of this article was to investigate and quantify this cancellation at $O(\alpha_s/(aM_Q))$. In our simulations we include all relevant current operators through dimension 4. The matching coefficients C_j have been calculated perturbatively through $O(\alpha_s/M_Q)$ and $O(a\,\alpha_s)$ [20]. Matrix elements of the dimension 4 current operators will contain in addition to Λ_{QCD}/M_Q physical contributions also power law terms of which the dominant $O(\alpha_s/(a\,M_Q))$ terms are cancelled by our matching coefficients. Remaining uncancelled power law terms start at $O(\alpha_s^2/(a\,M_Q))$ and their effects are taken into account in the systematic errors that we quote. Our analysis, based on the temporal component of the axial vector current, A_0, demonstrates that, although power law contributions are substantial there are no problems with cancelling them and there are no delicate fine tunings involved. Furthermore, we find that after cancellation of $O(\alpha_s/(aM_Q))$ terms the contributions from $1/M_Q$ current corrections are significantly reduced.

The third goal of the present study was to carry out other consistency tests in our lattice evaluation of f_{B_s}. The definition eq.(1) of the decay constant tells us that one should be able to obtain the same f_{B_s} from B_s mesons at rest and from those with nonzero spatial momentum up to lattice artifacts. We have simulated leptonic decays of B_s mesons with nonzero momenta to check this. Another project, which we will report on in a separate publication, is determining f_{B_s} from the spatial component A_k, providing a further covariance test of calculations with NRQCD heavy quarks [21].

In the next section we introduce the lattice actions and current operators used in our simulations. Section III presents results for f_{B_s} at the three lattice spacings and scaling plots. In section IV we consider cancellation of power law contributions and also discuss the slope of $f_{PS}\sqrt{M_{PS}}$ versus $1/M_Q$ as one leaves the static limit. On our coarsest lattice we are able to simulate NRQCD charm quarks and in section V we present results for the D_s meson decay constant f_{D_s} at this one value for the lattice spacing. We describe f_{B_s} extracted at nonzero momenta in section VI and section VII gives a brief summary of this article. In an

Appendix we provide a Table of heavy-light current matching coefficients covering a wider range of heavy quark masses than in [20].

II. THE LATTICE ACTION AND CURRENT OPERATORS

We used the NRQCD heavy quark action density given by,

$$\mathcal{L} = \overline{\psi}_t \psi_t - \overline{\psi}_t \left(1 - \frac{a\delta H}{2}\right)_t \left(1 - \frac{aH_0}{2n}\right)^n_t U_4^\dagger \left(1 - \frac{aH_0}{2n}\right)^n_{t-1} \left(1 - \frac{a\delta H}{2}\right)_{t-1} \psi_{t-1}, \tag{4}$$

where ψ denotes a two-component Pauli spinor, H_0 is the nonrelativistic kinetic energy operator,

$$H_0 = -\frac{\Delta^{(2)}}{2M_0}, \tag{5}$$

and δH includes relativistic and finite-lattice-spacing corrections,

$$\begin{aligned}\delta H = & -c_1 \frac{g}{2M_0} \boldsymbol{\sigma} \cdot \mathbf{B} \\ & + c_2 \frac{ig}{8(M_0)^2} (\nabla \cdot \mathbf{E} - \mathbf{E} \cdot \nabla) - c_3 \frac{g}{8(M_0)^2} \boldsymbol{\sigma} \cdot (\nabla \times \mathbf{E} - \mathbf{E} \times \nabla) \\ & - c_4 \frac{(\Delta^{(2)})^2}{8(M_0)^3} + c_5 \frac{a^2 \Delta^{(4)}}{24 M_0} - c_6 \frac{a(\Delta^{(2)})^2}{16n(M_0)^2}.\end{aligned} \tag{6}$$

In addition to all $1/M^2$ terms we have also included the leading $1/M^3$ relativistic correction as well as the discretization corrections appearing at the same order in the momentum expansion. For all three β values the NRQCD action was tadpole-improved using the plaquette definition of u_0 [22] and the c_i were set equal to unity. Table II lists the bare heavy quark masses aM_0 at which simulations were carried out together with the corresponding values for the stability parameter n.

For the light quarks we used the tree-level tadpole improved clover action ($c_{SW} = u_0^{-3}$) at $\beta = 5.7$ and $\beta = 6.0$. However at $\beta = 6.2$ the nonperturbatively determined value $c_{SW} = 1.61$ was employed [23]. The κ values used in the simulations are listed in Table I. At $\beta = 5.7$ and $\beta = 6.2$ we employed a single κ close to κ_s fixed through the K meson. At $\beta = 6.0$ data was obtained at three light κ's, 0.1369, 0.1375 and 0.13808, and results were then interpolated to κ_s [3]. In Table I. we also list the lattice spacing determined from the ρ mass and the bare dimensionless heavy quark mass aM_0^b corresponding to the b quark. The latter was determined from a combination of perturbation theory for mass renormalization and simulation results for binding energies. These procedures for fixing aM_0^b have been explained in several previous publications [3,15]. The simulation parameters given in this paragraph apply to results presented in sections III, IV and V. The $\beta = 6.0$ simulations described in section VI use different parameters (see section VI and Table VII).

For the temporal component of the heavy-light axial vector current eq.(2) becomes,

$$\langle\, A_0 \,\rangle_{QCD} = \sum_{j=0}^{2} C_j^{(A_0)} \langle\, J_0^{(j)} \,\rangle \;\; + \;\; O(1/M_Q^2), \tag{7}$$

with

$$\begin{aligned} J_0^{(0)} &= \bar{q}\,\gamma_5\gamma_0\, Q, \\ J_0^{(1)} &= \frac{-1}{2M_0}\bar{q}\,\gamma_5\gamma_0\,\boldsymbol{\gamma}\cdot\boldsymbol{\nabla}\, Q, \\ J_0^{(2)} &= \frac{1}{2M_0}\bar{q}\,\boldsymbol{\gamma}\cdot\overleftarrow{\boldsymbol{\nabla}}\;\gamma_5\gamma_0\, Q. \end{aligned} \tag{8}$$

The heavy quark 4-spinor Q has the NRQCD 2-spinor ψ as the upper two components, zero for the lower two components and obeys $\gamma_0 Q = Q$. $J_0^{(0)}$ and $J_0^{(1)}$ contribute already at tree-level whereas $J_0^{(2)}$ appears only at one-loop.

Higher dimension operators appear in lattice effective theories when one, for instance, needs to consider relativistic corrections. They also occur whenever lattice operators are improved. Improvements to current operators take on the form,

$$J_\mu^{(j)disc} = a^{l_j} O_\mu^{(j)}, \tag{9}$$

where again, as in eq.(3), the $O_\mu^{(j)}$ are operators of dimension $d_j = 3 + l_j$. In the present case of NRQCD-clover currents, one has the identical set of possible dimension 4 operators $O_\mu^{(j)}$ in eq.(3) and eq.(9). Hence a one-loop mixing and matching calculation to full continuum QCD involving the above $J_\mu^{(j)}$ will not only tell us how the $1/M_Q$ currents contribute but will also identify the discretization corrections that come in at one-loop. In other words a consistent matching through $O(\alpha_s/M_Q)$ should automatically be consistent through $O(a\,\alpha_s)$. In reference [20] it was found that for each μ only one of the $J_\mu^{(j)disc}$ was relevant at one-loop. Matching to continuum QCD could be achieved by improving $J_\mu^{(0)}$ in the following way,

$$J_\mu^{(0)} \quad \rightarrow \quad J_\mu^{(0)} + \alpha_s\, \zeta_{A_\mu}\, J_\mu^{(disc)}, \tag{10}$$

with

$$J_\mu^{(disc)} = -a\,\bar{q}\,\boldsymbol{\gamma}\cdot\overleftarrow{\boldsymbol{\nabla}}\;\gamma_0\gamma_5\gamma_\mu\, Q = 2aM_0\, J_\mu^{(2)}, \tag{11}$$

and $\zeta_{A_0} = 1.03$. The effect of $J_\mu^{(disc)}$ can be taken into account by expressing it in terms of $J_\mu^{(2)}$ and absorbing $\alpha_s 2aM_0\,\zeta_{A_\mu}$ into the coefficient $C_2^{(A_\mu)}$.

At $\beta = 5.7$ and $\beta = 6.0$ $1/M_Q^2$ current corrections that appear at tree-level have also been studied. For A_0 these are,

$$\begin{aligned} J_0^{(3)} &= \frac{1}{8M_0^2}\,\bar{q}\,\gamma_5\gamma_0\mathbf{D}^2\, Q, \\ J_0^{(4)} &= \frac{g}{8M_0^2}\,\bar{q}\,\gamma_5\gamma_0\boldsymbol{\Sigma}\cdot\mathbf{B}\, Q, \\ J_0^{(5)} &= \frac{-ig}{4M_0^2}\,\bar{q}\,\gamma_5\gamma_0\boldsymbol{\alpha}\cdot\mathbf{E}\, Q, \end{aligned} \tag{12}$$

where $\boldsymbol{\alpha} \equiv \gamma_0 \boldsymbol{\gamma}$ and $\boldsymbol{\Sigma} = diag(\boldsymbol{\sigma}, \boldsymbol{\sigma})$. We will comment on matrix elements of these currents and their M_Q dependence later in section V. However, since the $O(\alpha_s/M_Q^2)$ full matching calculation has not been carried out yet, $O(\alpha_s/(a\,M_Q)^2)$ and $O(\alpha_s(\Lambda_{QCD}/M_Q)/(a\,M_Q))$ power law contaminations contained in these matrix elements will not be cancelled and we prefer not to include them in our scaling analysis of f_{B_s}. In reference [3] tree-level contributions from (12) were included. The total effect was a $\sim 3\%$ decrease in f_{B_s}, well within the systematic errors quoted there for uncancelled power law terms. In the $\beta = 6.0$ results given in the present article, however, we have removed the $1/M_Q^2$ tree-level current effects.

Based on the lattice actions employed, the improvement of $J_\mu^{(0)}$ and the consistent matching to continuum full QCD through $O(\alpha_s/M_Q)$ and $O(a\,\alpha_s)$, one can now list the expected remaining dominant systematic errors in our evaluation of $\langle\, A_\mu \,\rangle_{QCD}$. These are collected in Table III and their size, in percent, estimated for each β. In making these estimates we use $\Lambda_{QCD} \sim 400 MeV$, $\alpha_s(\beta = 5.7) \sim 0.33$, $\alpha_s(\beta = 6.0) \sim 0.24$, $\alpha_s(\beta = 6.2) \sim 0.20$ and approximate aM_Q with aM_0^b of Table I. The α_s values are close to $\alpha_P(q^* = 1/a)$, where α_P is the coupling introduced in reference [24] closely related to α_V which is based on the heavy quark potential [25,22]. Discretization errors come in at $O((a\Lambda_{QCD})^2)$, relativistic errors at $O((\Lambda_{QCD}/M_Q)^2)$. We fold in perturbative errors separately for $O(\alpha_s^2)$ and $O(\alpha_s^2/(aM_Q))$ since these have different β dependence and also to indicate that perturbation theory will eventually break down for small aM_Q, i.e. for large enough β. We note that in the absence of tree-level $O(1/(M_Q^2)$ current matrix elements, there are no $O(\alpha_s/(aM_Q)^2)$ errors in our calculations. As long as the same action is used in both the simulations and the perturbative matchings, all $O(\alpha_s/(aM_Q)^j)$ terms cancel between matrix elements and matching coefficients. One sees that on the two finer lattices the perturbative errors are dominant whereas at $\beta = 5.7$ both perturbative and discretization errors are equally important. Table III also lists other systematic errors (uncertainty in κ_s and fixing of a^{-1} from the ρ mass) and the statistical errors in the f_{B_s} determinations. Not listed are uncertainties due to quenching. Recent studies indicate that these last corrections can be substantial, at the $10 \sim 25\%$ level [9–11].

III. SIMULATION RESULTS AND SCALING OF f_{B_s}

In this section we describe f_{B_s} calculated from A_0 and investigate scaling of this quantity. We start with simulation results for current matrix elements in lattice units before renormalization. Table IV summarizes our results at $\beta = 5.7$ and $\beta = 6.2$ for

$$a^{3/2}\, f^{(j)} \sqrt{M_{PS}} = \frac{a^{3/2}}{\sqrt{M_{PS}}} \langle 0|\, J_0^{(j)}\, |PS\rangle. \tag{13}$$

Data are presented for several heavy quark masses with the light quark mass fixed to κ_q of Table I. The corresponding simulation data for $\beta = 6.0$ can be found in [3]. The matrix elements were evaluated in the meson rest frame. $\langle\, J_0^{(2)}\,\rangle$ is identical to $\langle\, J_0^{(1)}\,\rangle$ in this frame and hence is not listed separately in the Table. For $\beta = 5.7$ we also list results for the higher order currents of eq.(12).

Results in physical units ($GeV^{3/2}$) for

$$f_{PS}\sqrt{M_{PS}} = \sum_{j=0}^{2} C_j^{(A_0)} f^{(j)} \sqrt{M_{PS}} \tag{14}$$

are summarized in Table V, at tree-level ($C_0^{(A_0)} = C_1^{(A_0)} = 1$, $C_2^{(A_0)} = 0$) and with one-loop matching for three different scales to fix $\alpha_s = \alpha_P(q^*)$. At $\beta = 5.7$ and $\beta = 6.0$ we can directly take over the matching coefficients from Appendix A, which assume tadpole improvement in both the NRQCD and clover actions. At $\beta = 6.2$ where the non-perturbative c_{SW} is used, some slight modifications are necessary. We first remove the tadpole improvement term coming from the light quark wave function renormalization (denoted C_q^{TI} in [20]) from the matching coefficients. We then use κ rather than $\tilde{\kappa} = \kappa \times u_0$ to rescale the light quark field in the currents. As a result the entries in Table IV and the tree-level results in Table V are enhanced for $\beta = 6.2$ by approximately a factor of $u_0^{-1/2}$. This enhancement is compensated for to a large extent upon going to renormalized matrix elements (the latter three columns in Table V) due to larger perturbative matching coefficients.

The scale q^* has not been calculated yet for the matching coefficients with NRQCD heavy and clover light quarks. q^* is known for static heavy quarks combined with massless Wilson light quarks [26] and also for light-light currents [27] again using massless Wilson fermions. These authors find $q^* = 2.18/a$ and $q^* = 2.3/a$ respectively, suggesting very mild dependence of q^* on aM_Q. Results also exist for clover light-light currents [28] showing some reduction in q^* relative to the Wilson results for these currents. In the absence of an explicit calculation for the action and currents employed in the present simulations, we use the $q^* = 2/a$ numbers to quote central values and arrange for perturbative errors to cover the spread in results due to uncertainty in q^*. Table VI shows our final numbers for f_{B_s} interpolated to the physical heavy quark mass M_0^b for the three lattice spacings. The Particle Data Group's B_s^0 mass, 5.369GeV, was used to convert from $f_{PS}\sqrt{M_{PS}}$ to f_{B_s}. The errors follow those listed in Table III and correspond from left to right to statistical (plus interpolation in M_0), discretization, perturbative, relativistic, κ_s determination and errors in $a^{-1}(m_\rho)$.

After adding all errors in quadrature, we plot f_{B_s} versus a in Fig. 1 and compare with results from [4]. One finds good scaling within errors and excellent agreement between the two collaborations. These results also agree well with quenched f_{B_s} determinations using other heavy fermion formulations on the lattice [1].

Table VI and Fig.1 represent one of the main results of this article. Working around a^{-1} of $\sim$ 2GeV with NRQCD-clover quarks and Wilson glue and matching through $O(\alpha_s/M_Q)$ and $O(a\,\alpha_s)$, one can obtain reliable quenched numbers for B meson decay constants with $\sim 10\%$ accuracy. To do better at these lattice spacings one would need to go to higher orders in the matching procedure. At our coarsest lattice spacing the systematic uncertainties are larger. Going to more highly improved actions would help here. Nevertheless, the $\beta = 5.7$ results are consistent with our best numbers. Simulations with $a^{-1} \sim$ 1GeV can already give a good indication of continuum physics.

Since we cannot extrapolate to $a \to 0$, in order to quote our best estimate for quenched f_{B_s} there are several choices. One approach would be to average over the $\beta = 6.0$ and $\beta = 6.2$ results. Alternatively one could, after having verified scaling behaviour, pick the point with the smallest statistical and systematic errors. Based on Table III this corresponds to the $\beta = 6.2$ result. We adopt the second method here and present as our final best value for the B_s meson decay constant in the quenched approximation,

$$f_{B_s} = 187(3)(4)(12)(2)(8)(6) \text{ MeV}, \tag{15}$$

with errors as described in Table VI.

If the value of f_{B_s} at the physical $b-$quark mass were our only goal then we would be done at this point. However, if further details are of interest, such as " the true size of contributions from $1/M_Q$ current corrections to f_B " or " the slope of $f_{PS}\sqrt{M_{PS}}$ versus $1/M_Q$ ", then one needs to scrutinize more carefully the contributions from individual current matrix elements $\langle J_0^{(j)} \rangle$ and matching coefficients C_j to the RHS of eq.(7). We turn to these issues in the next section.

IV. POWER LAW TERMS AND Λ_{QCD}/M_Q CORRECTIONS

In this section we investigate further the properties of matrix elements of the $1/M_Q$ current corrections. We focus on the current $J_0^{(1)} = \frac{-1}{2M_0}\bar{q}\,\gamma_5\gamma_0\,\boldsymbol{\gamma}\cdot\boldsymbol{\nabla}\,Q$. This operator is introduced in order to take into account p/M_Q effects which we know are present in the full theory, i.e. in the LHS of eq.(7). Here "p" is the momentum of the quarks inside the meson and should be of $O(\Lambda_{QCD})$. Once introduced into the effective theory, however, this current will mix with other currents in the theory. Its short distance effect will be to renormalize the zeroth order current and one expects the matrix element $\langle J_0^{(1)} \rangle$ to develop a component proportional to $\langle J_0^{(0)} \rangle$. On dimensional grounds the proportionality coefficient will be of the form $const/(a\,M_Q)$ and one has,

$$\langle J_0^{(1)} \rangle = \frac{C_{10}}{a\,M_Q}\langle J_0^{(0)} \rangle + \frac{\Lambda_{QCD}}{M_Q}\,term \qquad + \qquad higher\ orders. \tag{16}$$

The first term on the RHS of (16) is an example of a power law contribution to a matrix element. They are unavoidable in a quantum effective field theory where one has mixing between operators of different dimensions. However, the matching procedures between the full and the effective theories should remove these artifacts. Since we do the matching perturbatively, power law contributions can only be subtracted to a given order in α_s. As mentioned several times already, in our present calculations we cancel terms through $O(\alpha_s/(a\,M_Q))$. To see precisely how this cancellation comes about we need to dissect the matching coefficient $C_{j=0}$. Using the notation of [20] one can rewrite eq.(7) as,

$$\langle A_0 \rangle_{QCD} = (1 + \alpha_s\,\rho_0)\,\langle J_0^{(0)}\rangle + (1 + \alpha_s\,\rho_1)\,\langle J_0^{(1)}\rangle + \alpha_s\,\rho_2\ \langle J_0^{(2)}\rangle, \tag{17}$$

with

$$\rho_0 = B_0 - \frac{1}{2}(C_q + C_Q) - \zeta_{00} - \zeta_{10} \equiv \tilde{\rho}_0 - \zeta_{10}. \tag{18}$$

ρ_0 is the one-loop contribution to C_0 and consists of parts coming from continuum perturbation theory (B_0), from light and heavy quark wave function renormalizations on the lattice

(C_q and C_Q) and from mixing between the currents $J_0^{(j)}$ (ζ_{00} and ζ_{10}). ζ_{00} is the feedback of $J_0^{(0)}$ onto itself and ζ_{10} incapsulates the projection of $J_0^{(1)}$ back onto $J_0^{(0)}$, precisely what one is looking for in the first term of (16). Picking out the relevant terms, one can write

$$(1 + \alpha_s \rho_0) \langle J_0^{(0)} \rangle + \langle J_0^{(1)} \rangle = (1 + \alpha_s \tilde{\rho}_0) \langle J_0^{(0)} \rangle + \left[\frac{C_{10}}{a\, M_Q} - \alpha_s \zeta_{10} \right] \langle J_0^{(0)} \rangle + \frac{\Lambda_{QCD}}{M_Q}\, term\; + \;\ldots \tag{19}$$

The power law contribution $\left[\frac{C_{10}}{a\,M_Q} - \alpha_s \zeta_{10}\right] \langle J_0^{(0)} \rangle$ has now been reduced from an $O(\alpha_s/(a\,M_Q))$ to an $O(\alpha_s^2/(a\,M_Q))$ effect through the $\alpha_s \zeta_{10}$ matching term. It is convenient to define a subtracted $J_0^{(1)}$,

$$\langle J_0^{(1)} \rangle_{sub} = \langle J_0^{(1)} \rangle - \alpha_s \zeta_{10} \langle J_0^{(0)} \rangle, \tag{20}$$

which is equal to the second line in (19) up to higher order corrections. It is $\langle J_0^{(1)} \rangle_{sub}$ rather than $\langle J_0^{(1)} \rangle$ that should be used to assess the importance of $1/M_Q$ current corrections to f_{B_s}. In Fig.2 we plot the absolute values of $f^{(0)}\sqrt{M}$, $f^{(1)}\sqrt{M}$ and $f^{(1)}_{sub}\sqrt{M}$ (related to $\langle J_0^{(0)} \rangle$, $\langle J_0^{(1)} \rangle$ and $\langle J_0^{(1)} \rangle_{sub}$ in the usual way) versus $1/M_{PS}$ at $\beta = 6.0$. One sees that $|f^{(1)}_{sub}|\sqrt{M}$ is considerably smaller than $|f^{(1)}|\sqrt{M}$ and amounts to only $\sim 4\%$ to $\sim 5\%$ of the lowest order $f^{(0)}\sqrt{M}$ term. This is of the order of systematic errors such as $O(\alpha_s^2)$ errors remaining in our calculation, so we cannot give a more precise estimate of the true Λ_{QCD}/M_Q contributions coming from $1/M_Q$ currents. Similar results are obtained at the other lattice spacings. A corresponding plot similar to Fig.2 for $\beta = 5.7$ will be discussed in the next section. At all three β values the power law contributions make up 50% to 80% of $\langle J_0^{(1)} \rangle$, depending on q^*, and once they are subtracted away one is left with only a small remainder. We note that the subtraction in (20) took place automatically in the f_{B_s} calculations of the previous section. The fact that $f^{(1)}_{sub}\sqrt{M}$ turned out to be small did not pose any problems for the power law cancellation itself at $O(\alpha_s/(aM_Q))$.

Another quantity where having information on Λ_{QCD}/M_Q corrections is important, is the slope of $f_{PS}\sqrt{M_{PS}}$ versus $1/M_Q$. Writing,

$$f_{PS}\sqrt{M_{PS}} = \left(f_{PS}\sqrt{M_{PS}}\right)_{stat} [1 + \frac{\Lambda_{sl}}{M_Q} + O(1/M_Q^2)], \tag{21}$$

one is interested in the slope Λ_{sl}. The bulk of the effect will come from $1/M_Q$ terms in the NRQCD action which are responsible for the M_Q dependence of the zeroth order current matrix element $\langle J_0^{(0)} \rangle$, and from the one-loop correction $\tilde{\rho}_0$ to this matrix element. We have just seen that contributions from $1/M_Q$ current corrections are small. Nevertheless, when simulation data are fit to the form (21) to extract Λ_{sl} one might worry about contaminations due to uncancelled power law terms of $O(\alpha_s^2/(a\,M_Q))$. If Λ_{sl} is the result of a fit then one can estimate a percentage error of $\alpha_s^2/(a\,\Lambda_{sl})$ in this slope. Putting in some numbers this leads to $\frac{10\sim13}{\Lambda_{sl}[GeV]}\%$ uncertainties depending on β, where Λ_{sl} must be inserted in GeV's. If the slope is less than Λ_{QCD} (0.4 GeV) these errors can become quite large.

There is, however, another reason why it is difficult to extract an accurate Λ_{sl} from our simulations. In order to calculate the slope we need to look at data at masses larger than the b quark mass. The one-loop terms in the matching coefficients increase as one goes towards the static limit and as a consequence results for $f_{PS}\sqrt{M_{PS}}$ become much more sensitive to the value of α_s i.e. to q^*. This can be seen in Fig. 3 where $f_{PS}\sqrt{M_{PS}}$ is plotted versus $1/M_{PS}$ for $q^* = 1/a$ and $q^* = \pi/a$. One sees that there is considerable dependence of the slope on q^*. We will quote a central value for the slope based on the $\beta = 6.0$ data using $q^* = 2/a$ and allow for a change in q^* in our error. We note that in order for the expansion in (21) to be valid there should be only power dependence and no logarithmic dependence on M_Q. We satisfy this condition by fixing the logarithms in the matching coefficients to $\log(a\,M_0^b)$. Our best estimate for Λ_{sl} is then: $\Lambda_{sl} = -0.67(9)(^{-17}_{+34})(12)$GeV. The first error is the statistical fit error to the $q^* = 2/a$ data and the second comes from the upper limit of errors on the magnitude of the slope from fits to $q^* = \pi/a$ data and the lower limit of errors in fits to $q^* = 1/a$ data. The third error is an estimate for α_s^2 and $\alpha_s^2/(a\,M_Q)$ corrections. In Fig. 4 we plot the $\beta = 6.0$ results together with data from other β values all using $q^* = 2/a$. One sees that slopes extracted at the two finer lattice spacings are consistent within our large errors. Results from $\beta = 5.7$ lie mostly parallel to the $\beta = 6.0$ and $\beta = 6.2$ data, however statistical errors are too large near the static limit to enable a useful estimate for the slope. Around the physical B meson the $\beta = 5.7$ data points lie $\sim$15% high, in agreement with results in Table VI and consistent with our estimates of systematic errors in Table III.

In contrast to f_{B_s} which we demonstrated can be calculated with $\sim 10\%$ errors, we find that specific $1/M_Q$ corrections are harder to determine with comparable percentage accuracy. For the two quantities discussed in this section, the $1/M_Q$ corrections coming from the current corrections and the slope of $f_{PS}\sqrt{M_{PS}}$ as one leaves the static limit, the main reason is uncertainty coming from higher order perturbative corrections.

V. SIMULATIONS AT THE CHARM QUARK AND f_{D_s}

In this section we discuss the behaviour of the decay constant and the current matrix elements for heavy quark masses in the charm region. For the coarsest of our lattice spacings the charm quark can be reached at a bare mass of $a M_0^c = 0.87(6)(3)(^{+0}_{-13})$ [15].

The size of the lattice current matrix elements for different values of the heavy quark mass is compared in Fig.5 . This figure is similar to Fig.2, however at $\beta = 5.7$ we cover a much wider range of mass values. We also plot $1/M_Q^2$ current matrix elements. The figure shows the value of $|f_{sub}^{(1)}|\sqrt{M}$ to be subleading even in the charm region, however it has grown from 4% of $f^{(0)}\sqrt{M}$ at the B_s to 14% at the D_s. For $aM_Q \approx 1$ the value of the $1/M_Q^2$ current matrix element $(|f^{(3)} + f^{(4)} + f^{(5)}|)\sqrt{M}$ is equal to $|f^{(1)}|\sqrt{M}$ and the two lines in Fig.5 cross. After the discussion in the previous section, this is not unexpected and provides evidence that this current is also dominated by power law contributions. The part of the current $\langle J_0^{(3)} + J_0^{(4)} + J_0^{(5)}\rangle$ proportional to $\langle J_0^{(0)}\rangle$ diverges as $\alpha_s/(aM_Q)^2$. For $aM_0 \approx 1$ this results in a suppression of $\mathcal{O}(\alpha_s)$ with respect to $\langle J_0^{(0)}\rangle$, which is the same suppression factor as the one for $\langle J_0^{(1)}\rangle$. In order to avoid uncertainties of $\mathcal{O}(\alpha_s/(aM_Q)^2)$ in the final f_{D_s}, we do not include the matrix elements of $1/M_Q^2$ currents. By doing so, we have to accept an uncertainty of the size of Λ_{QCD}^2/M_Q^2, which is 10%, for the final result. This is a conservative estimate, however. Based on our experience with Λ_{QCD}/M_Q current corrections, we can expect that most of $(|f^{(3)}+f^{(4)}+f^{(5)}|)\sqrt{M}$ plotted in Fig.5 will eventually be cancelled by matching coefficients at $O(\alpha_s/(aM_Q)^2)$. So, even at the D_s, the true Λ_{QCD}^2/M_Q^2 current corrections should not be a large effect. The other Λ_{QCD}^2/M_Q^2 contributions in f_{D_s} come from the Λ_{QCD}^2/M_Q^2 terms in the NRQCD action, and these are already included in the present simulations.

For the perturbative uncertainties we assign 11% for α_s^2. This is larger than the uncertainty of f_{D_s} arising from the variation of q^* in a range from 1 to π. For the residual power law contributions of $\mathcal{O}(\alpha_s^2/aM_Q)$ we assign an uncertainty of 13%, which leads to 17% for the total perturbative error, when added in quadrature. The 13% uncertainty is comparable to the size of the entire $\langle J_0^{(1)}\rangle_{sub}$ matrix element. For the uncertainty in the strange quark mass we assign 4% as in the case of f_{B_s}, which turns out to be negligible compared to the other sources of uncertainty. It is interesting to note that the uncertainty arising from the scale $a(m_\rho)$ almost cancels between the effect this has on the conversion of the matrix element into physical units and the shift of the bare charm quark mass.

For our final result we obtain

$$f_{D_s} = 223(6)(29)(38)(23)(9)(^{+3}_{-1})\ \text{MeV} \qquad \rightarrow \qquad f_{D_s} = 223(54)\ \text{MeV}\,. \tag{22}$$

The uncertainties are listed in the same order as in Table III. This result is in very good agreement with the lattice average of 220^{+25}_{-20} MeV quoted in [29] for quenched f_{D_s}, however the uncertainty we assign is larger. It is also interesting to compare with direct experimental determinations of f_{D_s}. In a recent review article the authors of reference [30] present a world averaged experimental value of $f_{D_s} = (241\pm32)$MeV, which is very consistent with the lattice numbers.

VI. f_{B_s} FROM FINITE MOMENTUM MESONS

This section investigates the defining matrix element eq.(1) for nonzero spatial momentum $\vec{p}$ at two lattice spacings, $\beta = 6.0$ and $\beta = 6.2$. Our goal is not to calculate f_{B_s} more accurately than we have done in section III from B mesons at rest, but to test our ability to simulate hadrons at finite spatial momenta and obtain consistent results. At each β we work at one value for the heavy quark mass and we do not attempt to extrapolate to the physical b quark. Furthermore at $\beta = 6.0$ we use a different set of configurations from the previous sections. The new configurations and light propagators were provided by the UKQCD collaboration. In Table VII we summarise relevant action parameters.

We accumulated data for four nonzero momenta, (0,0,1), (0,1,1), (1,1,1) and (0,0,2) in units of $2\pi/aL$ averaging over all equivalent momenta $\pm p_x$, $\pm p_y$ etc. From the difference of falloff energies of meson correlations with and without momenta,

$$\delta E(p) \equiv E_{sim}(p) - E_{sim}(0), \tag{23}$$

one can use a relativistic dispersion relation to define a mass for the heavy meson, usually called M_{kin},

$$M_{kin} = (p^2 - \delta E^2)/(2\,\delta E). \tag{24}$$

Our first test is to check the extent to which M_{kin} is independent of p. This nonperturbatively determined mass can also be compared with another mass M_{pert} based on the perturbative pole mass for the b quark combined with an energy shift E_0 and simulation results for $E_{sim}(p=0)$,

$$M_{pert} = Z_m\, M_0 - E_0 + E_{sim}(0). \tag{25}$$

We use one-loop perturbation theory for Z_m and E_0. The one-loop coefficients and q^* for the combination $(Z_m M_0 - E_0)$ are given in [15]. In Table VIII we list results for M_{kin} and M_{pert} in lattice units. The errors in M_{kin} are statistical and for M_{pert} we give $O(\alpha_s^2)$ perturbative errors. The statistical errors in M_{pert} coming from $E_{sim}(0)$ are negligible compared to the perturbative errors. The quality of our signals for finite momentum mesons depended rather strongly on the smearings employed (see [15] for details of smearings). In some instances, e.g. in the $\beta = 6.0$ data, clearer signals were obtained for the highest momentum than for some of the lower ones. We believe this is because the smearings used were better suited for that momentum. For momentum (1,1,1), on the other hand, we could not extract any useful results at $\beta = 6.0$. Fig. 6 plots aM_{kin} versus the momentum and compares with aM_{pert}. M_{kin} is reasonably independent of p for the range considered and agrees with M_{pert} within $\sim 1\sigma$. The statistical errors at some of our data points, however, are still considerable for M_{kin} and they could be hiding systematic discretization corrections.

The next quantity of interest is the ratio of the decay matrix element for a heavy meson with momentum $\vec{p}$ to that of a heavy meson decaying at rest [31]. More specifically we consider,

$$\frac{\langle 0|A_0|PS\ ,\ \vec{p}\rangle/\sqrt{E(p)}}{\langle 0|A_0|PS\ ,\ \vec{p}=0\rangle/\sqrt{M_{PS}}} = \frac{\sqrt{E(p)}}{\sqrt{M_{PS}}}, \tag{26}$$

where $E(p)$ is the total energy of the meson. The RHS of eq.(26) is a very slowly rising function of p, never getting very much above 1 for the momenta involved. In our simulations we take the following expression for the LHS, working to the same order in $1/M_Q$ as in the previous sections.

$$R(p) \equiv \frac{\sum_{j=0}^{2} C_j^{(A_0)} \langle 0|J_0^{(j)}|\vec{p}\rangle/\sqrt{E(p)}}{\sum_{j=0}^{2} C_j^{(A_0)} \langle 0|J_0^{(j)}|\vec{p}=0\rangle/\sqrt{M_{PS}}}. \tag{27}$$

Whereas M_{kin}, discussed above, checks for the correct relativistic dispersion relation in the energies, $R(p)$ tests the p dependence of amplitudes. In Table IX we give results for $R(p)$. We also list $R^{(0)}(p)$, the analogous ratio using only the zeroth order current $J_0^{(0)}$,

$$R^{(0)}(p) \equiv \frac{\langle 0|J_0^{(0)}|\vec{p}\rangle/\sqrt{E(p)}}{\langle 0|J_0^{(0)}|\vec{p}=0\rangle/\sqrt{M_{PS}}}. \tag{28}$$

One sees only a small change at less than the 1σ level between $R(p)$ and $R^{(0)}(p)$. Most of the effect of one-loop matching and $1/M_Q$ current corrections is canceled in this ratio. In Fig.7

we plot $R(p)$ versus the momentum. The full line is the expected behaviour coming from the RHS of eq.(26). A single line suffices for the two β values, since the difference in M_{PS} is negligible. One sees that results consistent with continuum expectations are obtained up to momenta of about 1.2 GeV. Even for the largest momenta deviations are less than $\sim$8%.

VII. SUMMARY

In this article we presented further tests of f_{B_s} determinations using NRQCD heavy quarks and clover light quarks. We checked for scaling, studied the dependence on the momentum of the decaying B_s meson and also investigated cancellation of power law terms through $O(\alpha_s/(aM))$. At one value of the lattice spacing we were able to determine the D_s meson decay constant. Our best values for f_{B_s} and f_{D_s} are given in eq.(15) and eq.(22) respectively. Our results are in good agreement with other lattice determinations of these quantities. In the case of f_{D_s}, for which experimental measurements exist, we obtain a value consistent with the current experimental world average as given in [30].

ACKNOWLEDGMENTS

This work was supported by the DOE under DE-FG02-91ER40690, PPARC under GR/L56343, NATO under CRG/94259 and by NSF. Simulations were carried out at NERSC and at EPCC. We thank the UKQCD collaboration for providing many of the configurations and light propagators.

S.C. acknowledges a fellowship from the Royal Society of Edinburgh. J.Sh. would like to thank members of the theoretical physics group at the University of Glasgow for their hospitality during an extended visit. Support from a PPARC Visiting Fellowship PPA/V/S/1997/00666 is gratefully acknowledged.

APPENDIX A: MATCHING COEFFICIENTS FOR A_0

In Table X we collect matching coefficients for A_0, i.e. the ρ_0, ρ_1, ρ_2 and the mixing coefficient ζ_{10} defined in eq.(17) and eq.(18). This augments numbers given in reference [20] where, for the case of the full NRQCD action used in the present simulations, a smaller set of heavy quark masses was covered. The coefficient ρ_2 in Table X includes contributions from $J_0^{(disc)}$, as explained after eq.(11). We note that in the first article of reference [20] a different convention was used and ρ_2 there did not include $2aM_0\zeta_{A_0}$. The new convention adopted here is more in line with those employed in the second article of reference [20] for matching of A_k, V_0 and V_k.

REFERENCES

[1] S. Hashimoto, review talk given at *Lattice* '99, Nucl. Phys. Proc. Suppl. **83-84**, 3 (2000).
[2] JLQCD collaboration, S. Aoki *et al.*, Phys. Rev. Lett. **80**, 5711 (1998).
[3] A. Ali Khan *et al.*, Phys. Lett. **B427**, 132 (1998).
[4] JLQCD collaboration, K-I. Ishikawa *et al.*, Phys. Rev. **D61**:074501 (2000).
[5] A.X. El-Khadra *et al.*, Phys. Rev. **D58**:014506 (1998).
[6] MILC collaboration, C. Bernard *et al.*, Phys. Rev. Lett. **81**, 4812 (1998).
[7] APE collaboration, D. Becirevic *et al.*, Phys. Rev. **D60**:074501 (1999).
[8] UKQCD collaboration, C. Maynard *et al.*, Nucl. Phys. Proc. Suppl. **83-84**, 322 (2000).
[9] S. Collins *et al.*, Phys. Rev. **D60**:074504 (1999).
[10] CP-PACS collaboration, A. Ali Khan *et al.*, Nucl. Phys. Proc. Suppl. **83-84**, 265 (2000).
[11] CP-PACS collaboration, H. Shanahan *et al.*, Nucl. Phys. Proc. Suppl. **83-84**, 331 (2000).
[12] G.P.Lepage *et al.*, Phys. Rev. **D46**, 4052 (1992).
[13] A. El-Khadra, A. Kronfeld and P. Mackenzie, Phys. Rev. **D55**, 3933 (1997).
[14] UKQCD collaboration, H. Shanahan *et al.*, Phys. Rev. **D55**, 1548 (1997).
[15] J. Hein *et al.*, hep-ph/0003130, to appear in Phys. Rev. **D**.
[16] UKQCD collaboration, P.A. Rowland, PhD thesis, University of Edinburgh, 1997.
[17] M. Göckeler *et al.*, Phys. Rev. **D57**, 5562 (1998).
[18] J. Hein *et al.*, Nucl. Phys. Proc. Suppl. **73**, 366 (1999).
[19] S. Collins *et al.*, Nucl. Phys. Proc. Suppl. **83-84**, 271 (2000).
[20] C. Morningstar and J. Shigemitsu; Phys. Rev. **D57**, 6741 (1998), Phys. Rev. **D59**:094504 (1999).
[21] S. Collins *et al.*, in preparation
[22] G.P. Lepage and P.B. Mackenzie, Phys. Rev. **D48**, 2250 (1993).
[23] K. Jansen *et al.*, Phys. Lett. B**372**, 275 (1996).
[24] C.T.H. Davies *et al.*, Phys. Lett. **B345**, 42 (1995).
[25] S.J. Brodsky, G.P. Lepage and P.B. Mackenzie, Phys. Rev. **D28**, 228 (1983).
[26] O. Hernandez and B. Hill, Phys. Rev **D50**, 495 (1994).
[27] C. Bernard, M. Golterman and C. McNeile, Phys. Rev. **D59**:074506 (1999).
[28] M. Crisafulli, V. Lubicz and A. Vladikas, Eur. Phys. J. **C4**, 145 (1998).
[29] T. Draper, review talk given at *Lattice* '98, Nucl. Phys. Proc. Suppl. **73**, 43 (1999).
[30] F. Parodi, P. Roudeau and A. Stocchi, Nuovo Cim. **A112**, 833 (1999).
[31] Similar studies are reported in : J.N. Simone, Nucl. Phys. Proc. Suppl. **53**, 386 (1997).

TABLES

	$\beta = 5.7$	$\beta = 6.0$	$\beta = 6.2$
volume	$12^3 \times 24$	$16^3 \times 48$	$24^3 \times 48$
# configs	278	$102 \times 2_{trev}$	144
c_{SW}	1.567 (tad. imp.)	1.479 (tad. imp.)	1.61 (nonpert.)
$a^{-1}(m_\rho)$ (GeV)	$1.116(12)(^{+56}_{-0})$ [14]	1.92(7) [3]	$2.59(^{+6}_{-10})(^{+9}_{-0})$ [15–17]
aM_0^b	$4.20(25)(5)(^{+0}_{-24})$ [15]	2.22(11) [3]	$1.64(5)(^{+8}_{-5})(^{+0}_{-7})$ [15]
κ_q	0.1400	0.13755	0.1346
κ_s	0.1399(1) [16]	0.13755(13) [3]	0.13466(7) [16]

TABLE I. Simulation details for sections I through V. The errors on a^{-1} include statistical errors and those due to the chiral extrapolation of m_ρ. aM_0^b is the bare b-quark mass in lattice units determined from the B (or B_s) meson. κ_q gives the light quark mass for which results are presented here and κ_s is the actual strange κ for these β values based on the K meson. At $\beta = 6.0$ time reversed configurations were also used and results were interpolated to κ_s.

	$\beta = 5.7$																			
aM_0	20.0	12.5	10.0	8.0	6.0	5.0	4.0	3.5	3.15	2.75	2.45	2.2	2.0	1.7	1.5	1.3	1.125	1.0	0.8	0.6
n	1	1	1	1	1	2	2	2	2	3	3	3	3	4	4	5	6	6	8	10
	$\beta = 6.0$																			
aM_0			10.0			7.0			4.0			2.7			2.0			1.6		
n			1			1			1			2			2			2		
	$\beta = 6.2$																			
aM_0			4.5						2.5						1.44					
n			1						3						3					

TABLE II. Bare heavy quark masses and n-values

Source	$\beta = 5.7$	$\beta = 6.0$	$\beta = 6.2$
statistical	3	3	2
disc. $O((a\Lambda_{QCD})^2)$	13	4	2
pert. $O(\alpha_s^2)$, $O(\alpha_s^2/(aM))$	11	7	6
NRQCD $O((\Lambda_{QCD}/M)^2)$	1	1	1
κ_s	+4	+4	+4
$a^{-1}(m_\rho)$	$(^{+5}_{-1})$	4	3
Total	**18**	**10**	**8**

TABLE III. Estimates of the statistical and main systematic errors, in percent, in our values for f_{B_s}

aM_0	$a^{3/2}f^{(0)}\sqrt{M}$	$a^{3/2}f^{(1)}\sqrt{M}$	$a^{3/2}f^{(3)}\sqrt{M}$	$a^{3/2}f^{(4)}\sqrt{M}$	$a^{3/2}f^{(5)}\sqrt{M}$
			$\beta = 5.7$		
0.600	0.455(7)	-0.188(4)	-0.229(4)	0.1148(20)	-0.1463(24)
0.800	0.445(7)	-0.1448(27)	-0.1145(21)	0.0583(10)	-0.0763(12)
1.000	0.445(8)	-0.1204(24)	-0.0678(13)	0.0348(6)	-0.0470(8)
1.125	0.449(8)	-0.1105(23)	-0.0535(11)	0.0267(5)	-0.0369(7)
1.300	0.455(9)	-0.0992(22)	-0.0395(9)	0.0193(4)	-0.0274(6)
1.500	0.462(9)	-0.0893(21)	-0.0297(7)	0.0141(3)	-0.0205(4)
1.700	0.471(10)	-0.0820(20)	-0.0238(6)	0.01072(25)	-0.0161(4)
2.000	0.484(11)	-0.0731(19)	-0.0179(5)	0.00754(19)	-0.01170(27)
2.200	0.492(11)	-0.0685(18)	-0.0153(4)	0.00616(17)	-0.00975(23)
2.450	0.503(12)	-0.0636(18)	-0.0130(4)	0.00490(14)	-0.00795(19)
2.750	0.515(13)	-0.0587(17)	-0.0108(3)	0.00385(12)	-0.00639(15)
3.150	0.528(14)	-0.0533(16)	-0.00874(25)	0.00289(10)	-0.00493(12)
3.500	0.541(15)	-0.0495(16)	-0.00748(23)	0.00233(9)	-0.00405(10)
4.000	0.556(17)	-0.0450(16)	-0.00614(20)	0.00177(7)	-0.00315(8)
5.000	0.583(21)	-0.0381(15)	-0.00440(16)	0.00112(5)	-0.00207(6)
6.000	0.602(25)	-0.0331(15)	-0.00331(13)	0.00077(5)	-0.00146(4)
8.000	0.64(3)	-0.0263(15)	-0.00213(10)	0.00043(3)	-0.00085(3)
10.000	0.66(4)	-0.0218(14)	-0.00149(9)	0.000272(25)	-0.000555(25)
12.500	0.68(6)	-0.0180(14)	-0.00103(7)	0.000171(19)	-0.000362(20)
20.000	0.73(9)	-0.0119(13)	-0.00045(4)	0.000066(11)	-0.000144(11)
			$\beta = 6.2$		
1.440	0.143(2)	-0.0195(3)			
2.500	0.147(2)	-0.0125(2)			
4.500	0.152(1)	-0.0076(1)			

TABLE IV. Matrix elements of individual current contributions in lattice units. $f^{(j)}$ is defined in eq. (13). The $\beta = 6.2$ matrix elements have different normalization from those at other β's (see text).

aM_0	tree-level	$q^* = 1/a$	$q^* = 2/a$	$q^* = \pi/a$
		$\beta = 5.7$		
0.600	0.315(6)	0.263(5)	0.280(5)	0.286(5)
0.800	0.353(6)	0.280(5)	0.304(5)	0.312(5)
1.000	0.382(7)	0.302(5)	0.328(6)	0.337(6)
1.125	0.399(7)	0.314(6)	0.341(6)	0.351(6)
1.300	0.419(8)	0.329(6)	0.358(7)	0.369(7)
1.500	0.440(9)	0.345(7)	0.375(8)	0.386(8)
1.700	0.459(10)	0.364(8)	0.394(9)	0.406(9)
2.000	0.484(11)	0.378(9)	0.412(10)	0.424(10)
2.200	0.500(11)	0.385(9)	0.422(10)	0.435(10)
2.450	0.518(12)	0.396(10)	0.435(10)	0.449(11)
2.750	0.538(14)	0.408(10)	0.450(11)	0.465(12)
3.150	0.560(15)	0.421(12)	0.466(13)	0.482(13)
3.500	0.579(17)	0.432(13)	0.479(14)	0.496(14)
4.000	0.603(19)	0.446(14)	0.496(16)	0.514(16)
5.000	0.642(24)	0.471(18)	0.526(19)	0.546(20)
6.000	0.671(28)	0.488(21)	0.547(23)	0.568(24)
8.000	0.72(4)	0.519(28)	0.58(3)	0.61(3)
10.000	0.75(5)	0.55(4)	0.61(4)	0.64(4)
12.500	0.79(7)	0.57(5)	0.64(6)	0.67(6)
20.000	0.84(10)	0.63(9)	0.70(10)	0.72(10)
		$\beta = 6.0$		
1.600	0.442(13)	0.398(11)	0.410(11)	0.414(11)
2.000	0.466(13)	0.406(13)	0.421(13)	0.427(13)
2.700	0.495(19)	0.421(16)	0.440(16)	0.448(16)
4.000	0.521(19)	0.442(16)	0.465(16)	0.473(16)
7.000	0.588(16)	0.479(13)	0.508(13)	0.518(13)
10.000	0.615(16)	0.498(13)	0.528(13)	0.540(13)
		$\beta = 6.2$		
1.440	0.515(8)	0.404(4)	0.429(8)	0.442(8)
2.500	0.561(8)	0.465(6)	0.485(6)	0.495(6)
4.500	0.602(4)	0.505(5)	0.527(5)	0.536(5)

TABLE V. Decay matrix elements $f\sqrt{M}$ in $GeV^{3/2}$. The first column gives tree-level results, the remaining columns include renormalization constants using α_P at three values of q^*. Only statistical errors are shown.

β	f_{B_s} in MeV		
5.7	$217(7)(28)(25)(2)(9)(^{+12}_{-3})$	$\to$	$217(^{+41}_{-39})$
6.0	184(7)(7)(13)(2)(7)(7)	$\to$	184(19)
6.2	187(3)(4)(12)(2)(8)(6)	$\to$	187(16)

TABLE VI. Quenched f_{B_s} with errors listed separately and added in quadrature to the right. The errors denote from left to right statistical (plus interpolations in M_0), discretization, perturbative, relativistic, fixing κ_s and a^{-1}.

	$\beta = 6.0$	$\beta = 6.2$
volume	$16^3 \times 48$	$24^3 \times 48$
# configs	268	144
c_{SW}	1.77 (nonpert.)	1.61 (nonpert.)
aM_0	2.0	1.44
κ_q	0.13344	0.1346

TABLE VII. Simulation details for section VI.

	$\beta = 6.0$	$\beta = 6.2$
aM_{pert}	2.53(8)	1.88(5)
aM_{kin}		
(0,0,1)	2.51(23)	1.93(33)
(0,1,1)	2.83(36)	1.77(19)
(1,1,1)	—–	1.73(17)
(0,0,2)	2.49(11)	1.63(16)

TABLE VIII. aM_{kin} extracted from pseudoscalar mesons with different momenta and comparison with aM_{pert}. Momenta are given in units of $2\pi/aL$. Values for the lowest momenta in lattice units are: $ap = 0.39$ ($\beta = 6.0$) and 0.26 ($\beta = 6.2$).

	$\beta=6.0$		$\beta=6.2$	
momentum	$R(p)$	$R^{(0)}(p)$	$R(p)$	$R^{(0)}(p)$
(0,0,1)	1.02(2)	1.01(2)	1.01(2)	1.00(2)
(0,1,1)	1.00(5)	0.98(5)	1.03(3)	1.02(3)
(1,1,1)	—	—	1.05(4)	1.03(4)
(0,0,2)	1.08(3)	1.05(3)	1.10(6)	1.07(6)

TABLE IX. The ratios $R(p)$ and $R^{(0)}(p)$ of eq.(27) and eq.(28) for several momenta and β values. Momenta are given in units of $2\pi/aL$.

aM_0	n	ρ_0	ρ_1	ρ_2	ζ_{10}
0.600	10	0.1875(6)	0.705(3)	0.487(2)	-0.9944(3)
0.800	8	-0.1191(4)	0.213(2)	0.758(2)	-0.7968(2)
0.800	5	-0.1203(4)	0.261(2)	0.680(2)	-0.7682(2)
1.000	6	-0.2207(3)	0.026(2)	0.914(2)	-0.6645(1)
1.000	4	-0.2108(3)	0.045(2)	0.849(2)	-0.6502(1)
1.125	6	-0.2546(3)	-0.035(2)	1.026(2)	-0.6063(1)
1.200	3	-0.2500(3)	-0.031(2)	0.987(3)	-0.5613(1)
1.300	5	-0.2814(3)	-0.068(2)	1.156(3)	-0.5387(1)
1.400	3	-0.2806(3)	-0.070(2)	1.187(3)	-0.5014(1)
1.440	3	-0.2855(3)	-0.071(2)	1.227(3)	-0.4909(1)
1.500	4	-0.2987(3)	-0.080(2)	1.324(3)	-0.4790(1)
1.500	2	-0.2732(3)	-0.061(2)	1.193(3)	-0.4675(1)
1.600	2	-0.2845(2)	-0.065(2)	1.311(4)	-0.4463(1)
1.700	2	-0.2941(2)	-0.064(2)	1.425(4)	-0.4267(1)
2.000	2	-0.3146(2)	-0.046(2)	1.781(4)	-0.3768(1)
2.500	3	-0.3382(2)	-0.006(2)	2.454(6)	-0.31626(7)
2.500	2	-0.3331(2)	-0.001(2)	2.432(6)	-0.31525(7)
2.700	2	-0.3374(2)	0.018(2)	2.706(6)	-0.29599(6)
3.000	2	-0.3421(2)	0.044(2)	3.132(7)	-0.27122(6)
3.500	2	-0.3457(2)	0.094(2)	3.895(8)	-0.23818(6)
4.000	2	-0.3460(2)	0.135(2)	4.705(10)	-0.21235(5)
4.000	1	-0.3374(2)	0.140(2)	4.600(10)	-0.21147(5)
4.500	1	-0.3379(2)	0.176(3)	5.467(11)	-0.19115(5)
5.000	1	-0.3362(2)	0.211(3)	6.328(12)	-0.17433(4)
7.000	1	-0.3173(2)	0.321(4)	10.050(21)	-0.12898(3)
10.000	1	-0.2770(2)	0.432(6)	15.957(30)	-0.09282(3)
12.500	1	-0.2432(2)	0.505(7)	20.905(36)	-0.07523(2)
20.000	1	-0.1528(2)	0.655(12)	36.335(64)	-0.04797(1)

TABLE X. One-loop matching coefficients ρ_0, ρ_1 and ρ_2 of eq.(17) and mixing coefficient ζ_{10} of eq.(18) for several heavy quark mass values. ρ_2 includes $2aM_0\,\zeta_{A_0}$ in order to incorporate contributions from $J^{(disc)}$. The NRQCD action is that of eq.(4) - (6) with $c_i = 1$. Both the NRQCD and clover light quark actions are taken to be tadpole-improved with the plaquette definition of u_0.

FIGURES

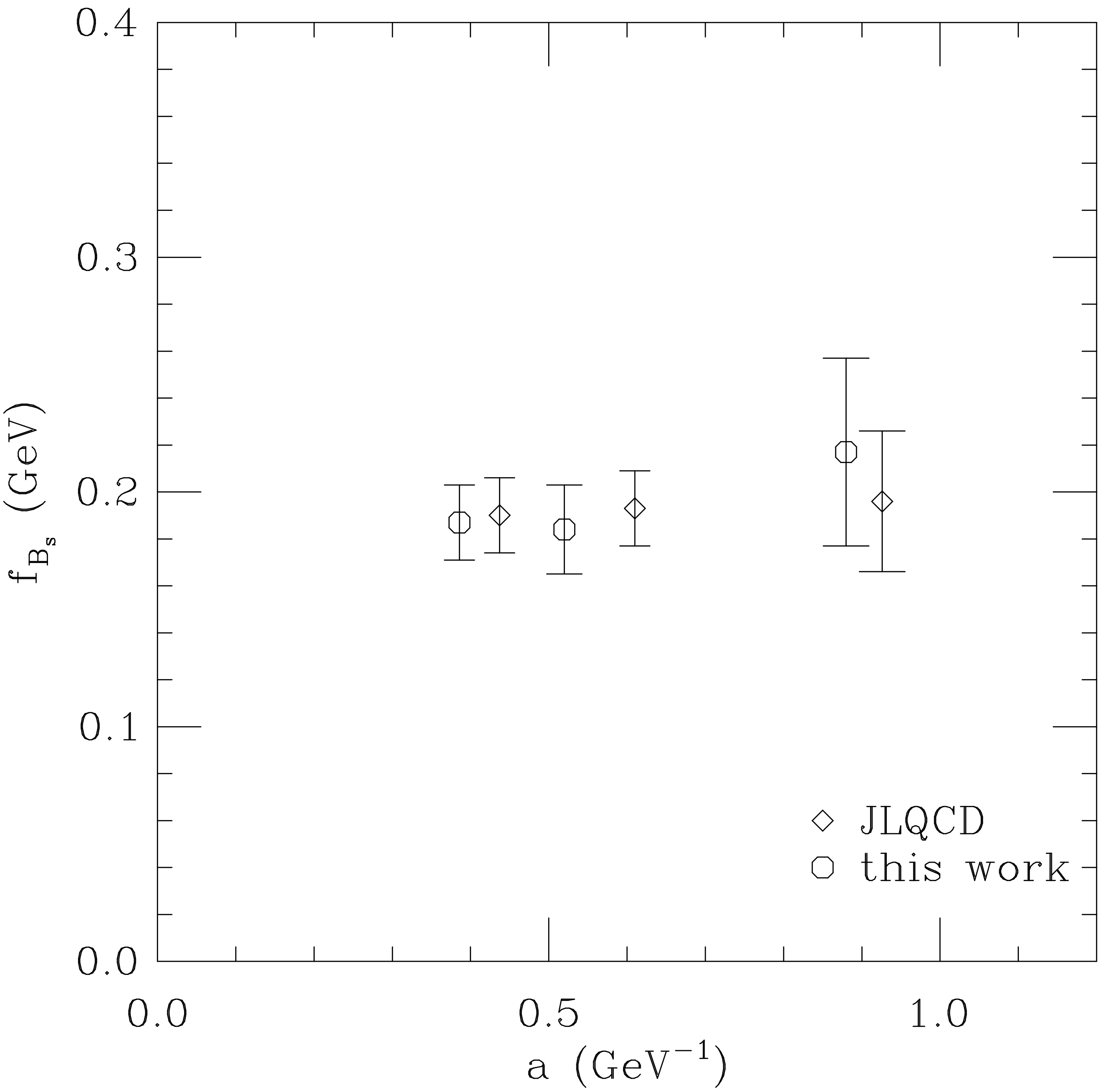

FIG. 1. f_{B_s} versus the lattice spacing and comparison with reference [4]. Systematic and statistical errors have been added in quadrature.

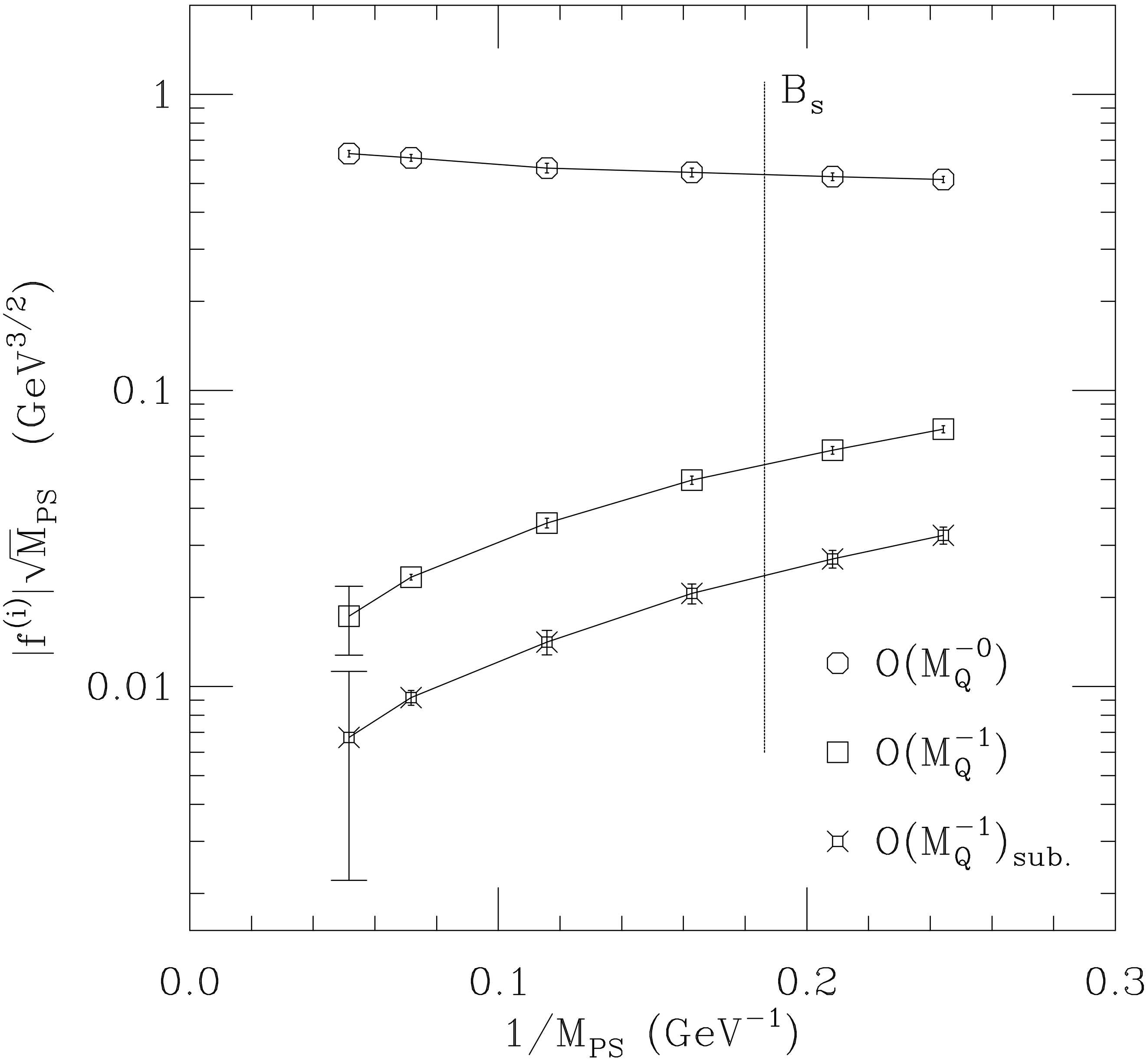

FIG. 2. Matrix elements $f^{(0)}\sqrt{M}$, $|f^{(1)}|\sqrt{M}$ and $|f^{(1)}_{sub}|\sqrt{M}$ versus $1/M_{PS}$ at $\beta = 6.0$. $q^* = 2/a$ was used to obtain $|f^{(1)}_{sub}|\sqrt{M}$.

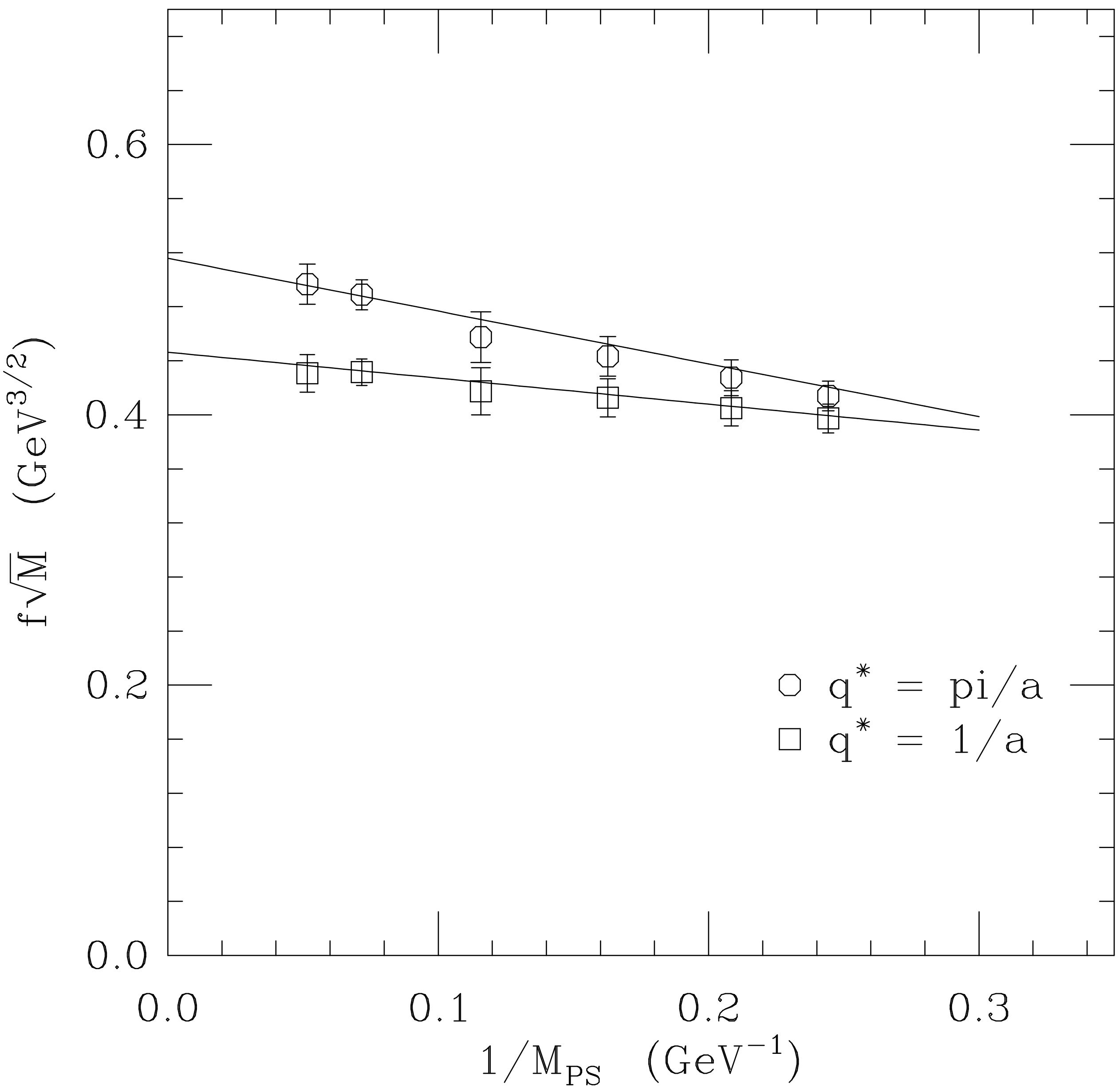

FIG. 3. $f_{PS}\sqrt{M_{PS}}$ versus $1/M_{PS}$ at $\beta = 6.0$ for $q^* = \pi/a$ and $q^* = 1/a$. The lines are linear fits to the data. Only statistical errors are shown.

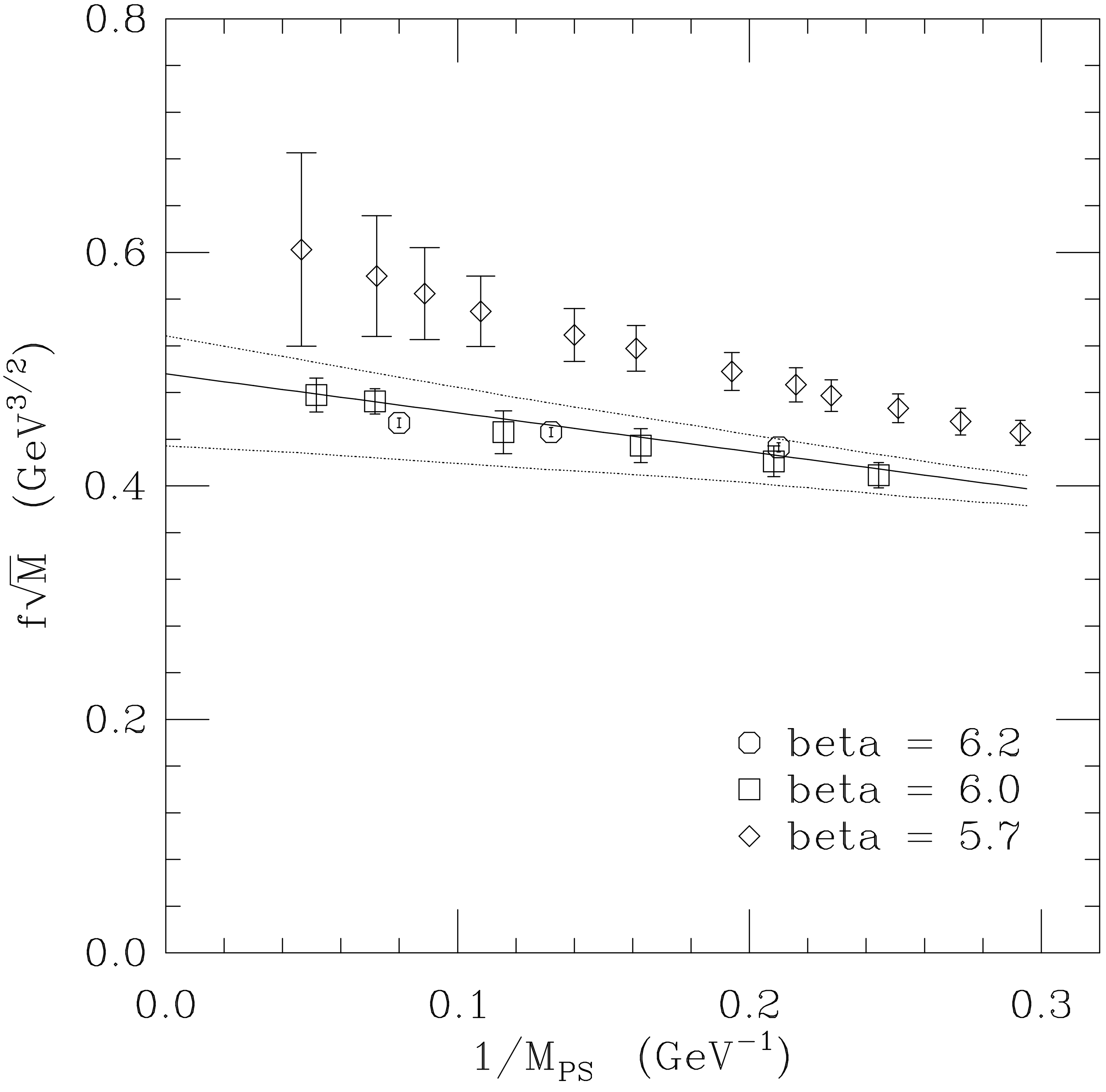

FIG. 4. Results for $f_{PS}\sqrt{M_{PS}}$ versus $1/M_{PS}$ from different β's. $q^* = 2/a$ is used for the one-loop renormalized data points. The central full line is a linear fit to the $q^* = 2/a$, $\beta = 6.0$ data. The bottom(top) dotted line comes from lower(upper) bounds on fits to $q^* = 1/a(q^* = \pi/a)$, $\beta = 6.0$ data (see text).

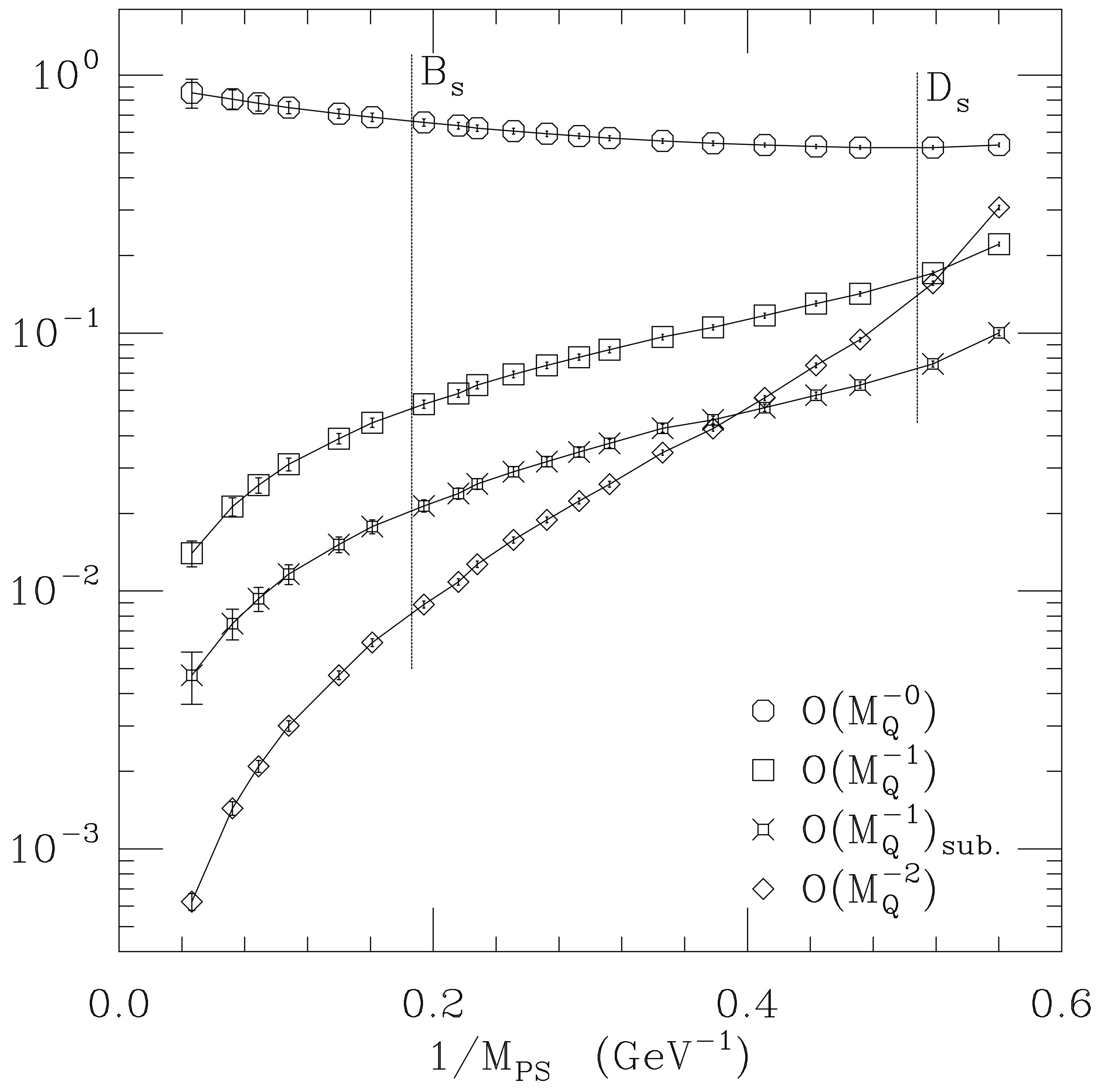

FIG. 5. Matrix elements $f^{(0)}\sqrt{M}$, $|f^{(1)}|\sqrt{M}$, $|f^{(1)}_{sub}|\sqrt{M}$ and $(|f^{(3)}+f^{(4)}+f^{(5)}|)\sqrt{M}$ versus $1/M_{PS}$ at $\beta=5.7$. $q^*=2/a$ was used to obtain $|f^{(1)}_{sub}|\sqrt{M}$.

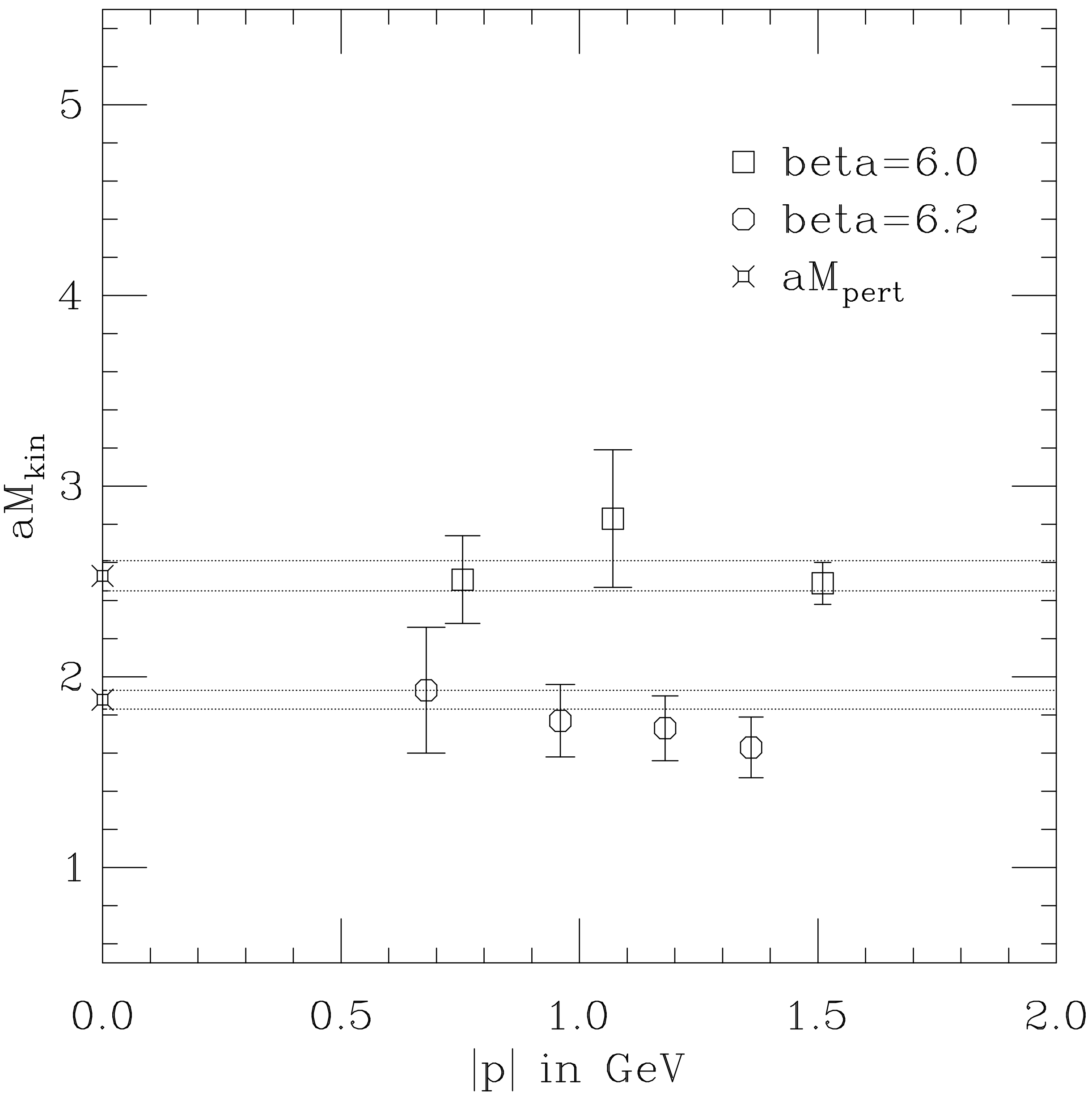

FIG. 6. aM_{kin} extracted from mesons with different spatial momenta. The fancy squares to the left show aM_{pert}. The horizontal lines bracket perturbative errors on aM_{pert}.

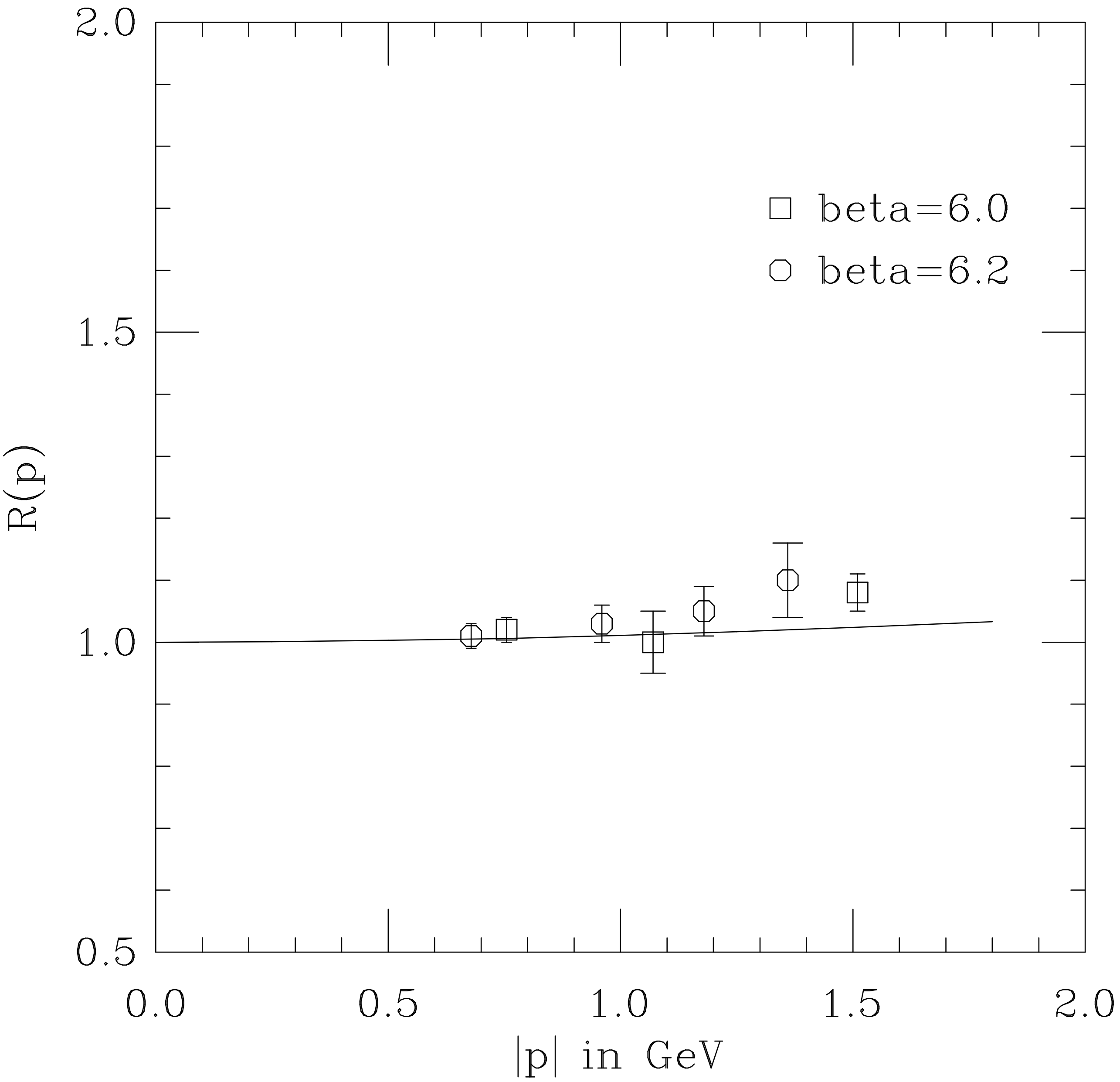

FIG. 7. The ratio $R(p)$ of eq.(27) versus momentum. The full line shows $\sqrt{E(p)}/\sqrt{M_{PS}}$.